Numerical Estimation of Hearth Internal Geometry of an Industrial Blast Furnace

Zhang, Chengbo; Chenxi, Zhao; Shao, Lei; Saxén, Henrik; Yingxia , Qu; Zou, Zongshu

Published in:
Steel Research International

DOI:
10.1002/srin.202100364
10.1002/srin.202100364

Published: 22/09/2022

Document Version
Accepted author manuscript

Numerical Estimation of Hearth Internal Geometry of an Industrial Blast Furnace

Chengbo Zhang,[1] Chenxi Zhao,[1] Lei Shao,[1*] Henrik Saxén,[2] Yingxia Qu[1] and Zongshu Zou[1]

[*]Corresponding author: shaolei@mail.neu.edu.cn

1. School of Metallurgy, Northeastern University, Shenyang 110819, China.
2. Process and Systems Engineering Laboratory, Åbo Akademi University, Åbo FI-20500, Finland

Abstract: Since the campaign of a modern blast furnace (BF) is usually restricted by its hearth integrity, monitoring the hearth internal geometry is of crucial importance for strategic operation planning. In order to provide an overall picture of the hearth inner geometry of a large-scale BF in a Chinese steelworks, a wear model based on the solution of an inverse heat-conduction problem was developed. Using the wear model, the evolutions of erosion and skull lines in the hearth were tracked for the period from the blow-in of the BF to its present state. The main findings are outlined in the present paper, where a detailed analysis and discussion of some observations are made to gain a deep understanding of the internal state of the hearth. A correlation between the thickness of the estimated skull layer and taphole length is demonstrated. The results indicate that the skull layer in the bottom of the BF hearth is much thicker than that in the sidewall and that lining erosion of the hearth mainly occurs in the sidewall. In addition, a thicker skull layer preventing the sidewall from excessive lining erosion correlates well with a longer taphole.

Keywords: blast furnace hearth, internal geometry, lining erosion, skull buildup, taphole length

1. Introduction

The campaign of a modern blast furnace (BF) is mainly limited by the integrity of its lower part, the hearth, where the lining refractories are exposed to an extremely hostile environment and thus inevitably eroded by a variety of chemical and mechanical mechanisms.[1-4] In the practical operation, the hearth walls are routinely cooled with surface or embedded water circuits and the liquid iron ("hot metal") in the vicinity of the hot face may therefore solidify to form a build-up ("skull") layer acting as an autogenous barrier to protect the remaining lining.[5, 6] However, an excessive growth of skull is detrimental since it reduces the effective hearth volume and consequently the possibilities to maintain a high production rate. Timely monitoring and proper control of the hearth internal geometry reflecting the state of lining erosion and skull buildup are, therefore, essential steps towards a successful BF operation with a long campaign and a high production rate.

The hearth internal geometry also evolves due to the varying state of the deadman, which is known to impose strong influence on the flow conditions of liquid iron and thus heat transfer process governing the skull formation and erosion behaviors.[7] Since direct online measurements in the hearth are still impossible, the temperatures measured by thermocouples placed in the hearth lining are usually utilized to estimate the internal geometry. For this, a number of hearth wear models based on the solution of an inverse heat-conduction problem have been reported in the literature over the years.[8-12] Some of these models have been implemented in industrial BFs, as well as been validated in different ways. For instance, the model developed by Brännbacka and Saxén was indirectly verified by correlating its results with independent hearth measurements during the furnace campaign,[9] while the model built by Zagaria and co-authors was validated by comparing the estimated hearth internal geometry with the actual one

measured at the blow-out of a BF.[10] In this category of models, at least two-dimensional domains are considered to consider the complicated layout of the BF hearth lining. The calculation of the internal profiles of skull layer (i.e., skull line) and remaining hearth lining (i.e., erosion line) is based on the commonly accepted procedure of estimating the location of the 1150 °C isotherm in the hearth lining: Carbon saturated pig iron cannot exist below this temperature in liquid form, so this isotherm corresponds to the maximum liquid iron penetration in the hearth lining.[8-10] The internal profiles of skull line and erosion line are then "reconstructed" by solving an optimization problem, where the difference between lining temperatures measured by thermocouples and simulated by the model is minimized. The model detects the inner profile of the intact lining by matching the most severe erosion experienced during the campaign. Later points corresponding to less severe erosion are taken as indications of skull formation on the intact lining. The estimated skull and erosion lines can be used as a basis for an assessment of the need to adjust the operation state to protect the lining or to avoid excessive skull growth. However, it should be noted that is still a non-trivial task to accurately identify the skull and erosion lines, particularly for scenarios where the historical thermocouple signals are not available for the whole furnace campaign or where the signal quality is low. The results of wear models can also be used for more sophisticated purposes. Kaymak and co-authors presented a multi-physics platform for monitoring the state of the BF hearth that in addition to estimating the hearth internal geometry can be used to analyze thermal stresses and deformation of the hearth lining and steel shell during the furnace campaign.[12] This model does not seem to apply any regularization term in the objective function, which may result in physically unrealistic estimates of the internal geometry. Still, this kind of versatile platform represents the direction of development of advanced monitoring and diagnosis tools for the BF hearth.

In order to provide an overall picture of the hearth internal geometry for a large-scale BF in a Chinese steelworks, a hearth wear model was developed, following the modeling concepts and numerical treatment proposed in [9]. The model automatically tracks the evolutions of the erosion and skull lines in the hearth based on thermocouple information from the lining. The information provided by the model serves as an aid in the BF operation to gain insight into the complex hearth phenomena and how the hearth state evolves in time as a result of changes in the operation conditions. This paper outlines some modelling results and correlates some of the findings with other process variables, such as taphole length, which are known to reflect the state of the hearth. Finally, some conclusions are presented and lines of future development are proposed.

2. Description of the Hearth and the Wear Model

2.1 The Blast Furnace and its Hearth

The BF studied in the present work has an inner volume of approximately 2500 m^3 and a target campaign of 15 years. It was blown in on June 26, 2012 and until today, the average rates of production, coke and (pulverized) coal consumption are about 6000 $tHM\ day^{-1}$, 390 $kg\ tHM^{-1}$ and 160 $kg\ tHM^{-1}$, respectively. The BF is equipped with a bell-less charging equipment at the top and its iron-bearing feedstock mainly consists of 70% sinter and 30% pellets. However, a minor fraction of imported lump ore is occasionally used. It is interesting to note that the content of titanium (Ti) in the feedstock is around 0.5% since this element commonly appears in the local iron ore to a relatively high amount. Oxygen-enriched (normally < 4%) hot blast with a temperature ranging between 1150 °C and 1200 °C is blown into the furnace through 30 tuyeres installed uniformly circumferentially at the lower part of the bosh (cf. Figure 1a). Some key design parameters of the BF are listed in Table 1, where the ratio of sump depth to hearth diameter is 19.3%. This value is fairly close to the critical one (i.e.,

20%) at which the deadman is believed to (at least partially) float in the BF hearth.[7, 13, 14] If the deadman partially floats, its bottom may assume a profile with higher floating levels near the hearth sidewall: this bottom shape has been confirmed in a set of quenched furnaces with a resembling sump depth.[15]

Table 1. Key design parameters of the blast furnace studied

Parameter	Value [m]
Effective furnace height	28.8
Throat height	2.0
Throat diameter	8.1
Belly height	2.0
Belly diameter	12.8
Bosh height	3.4
Hearth height	4.6
Hearth diameter	11.4
Sump depth	2.2

Figure 1a provides a three-dimensional sketch of the BF hearth structure, while the top view of the horizontal cross-section at the tuyere level (cf. A-A in panel a) is shown in Figure 1b. As depicted in panel a, the BF hearth is constructed of different high-conducting carbon bricks and a complete low-conducting ceramic cup. The specific refractories I-VI in the figure are microporous carbon brick, super-micropore carbon brick, graphite carbon brick, ramming material, corundum-mullite brick, as well as mullite brick, respectively. The lowermost dots in the bottom denote a set of cooling pipes where industrial demineralized water circulates. In panel b, the eight vertical sections (S1-S8) indicated by dashed lines denote locations where a (sufficient) set of

thermocouples are embedded in the hearth lining. It is also seen that the hearth has three tapholes, TH1-TH3, where TH1 and TH2 are located 139° and 221° with respect to TH3 in the clockwise direction. Normally, one of the three tapholes is plugged for maintenance (or is idle) and alternate tapping of the two other tapholes is applied, by switching practically continuously between them. The duration of a tap is usually kept around 2.5 h and after a couple of weeks, one of the operating tapholes is replaced by the idle taphole.

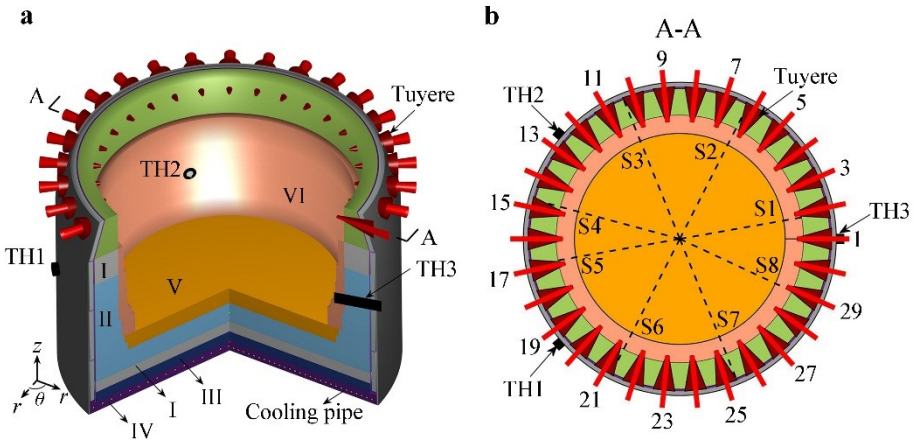

Figure 1. Structure of the blast furnace hearth: (a) three-dimensional sketch; (b) top-view from the horizontal cross-section at the tuyere level.

2.2 The Hearth Wear Model

By introducing steady-state assumption and neglecting the heat conduction in the angular direction (i.e. θ in Figure 1a), the wear model detects the erosion and skull lines in a series of two-dimensional vertical slices (i.e., computational domains) of the hearth, and interpolates the results into a three-dimensional representation of the entire region under consideration. The temperature field of each slice can be calculated by (numerically) solving the following partial differential equation with specifying appropriate boundary conditions.

$$\frac{1}{r}\frac{\partial}{\partial r}\left(\lambda r\frac{\partial T}{\partial r}\right)+\frac{\partial}{\partial z}\left(\lambda\frac{\partial T}{\partial z}\right)=0 \tag{1}$$

where T and λ are the temperature and thermal conductivity of the hearth lining (including skull), and r and z stand for the radial and axial coordinates. The calculated temperature field is then compared to thermocouple readings at some reference points. An inverse problem is therefore defined as finding the optimal shape of 1150 °C isotherm that yields the minimum difference between the calculated and measured temperatures at the reference points. In order to facilitate mathematical implementation, the shape of 1150 °C isotherm is parameterized using the method of direction vectors and to avoid physically unlikely solutions, a scaled regularization is taken into account in the objective function, E, expressed as

$$E=\sum_{i=1}^{M}\left(T_i^{\mathrm{c}}-T_i^{\mathrm{m}}\right)^2+\gamma\sum_{j=1}^{N}\left(\alpha_j-\tilde{c}_{,,}\right)^{`2} \tag{2}$$

where superscripts ‘c’ and ‘m’ represent the calculated and measured temperatures (at the M reference points). The second term on the right-hand side is the regularization basically concerning the internal geometry of the original (intact) hearth lining.[9]

In a straightforward procedure, iterative calculation is usually required to solve the inverse problem and the shape of 1150 °C isotherm needs to be adjusted in every iteration by generating a new computational mesh. However, this is known to be time-consuming and may induce numerical noise in the solution. In order to overcome these drawbacks, the present wear model applies the novel procedure originally developed by Brännbacka and Saxén.[9] In the procedure, the inverse problem is transformed into optimizing a set of thermal conductivities of a composite layer including the skull layer and an erosion reserve zone. The computational mesh therefore retains ‘fixed’ during iterative calculation. According to the conservation of local flux of one-dimensional

heat conduction, the optimal thermal conductivities are finally converted back to a set of skull layer and erosion zone thicknesses, which, in turn, are used for construction of skull and erosion lines. For the sake of brevity, other information about the present wear model is not presented here: the reader is referred to [9] for more details regarding the modelling concept and numerical treatment, as well as the validation.

As for the two-dimensional computational domains of the hearth, it is natural to choose them on the basis of S1-S8 (shown in Figure 1b) where a sufficient set of thermocouples are embedded in the hearth lining. As an example, the domain D1 selected on the basis of S1 is illustrated in Figure 2, where the computational mesh, consisting of about 1300 triangular cells, is arranged in a way that the resolution is higher in the region where the temperature varies greatly, i.e., the skull layer between the skull and erosion lines, as well as the residual ceramic cup.

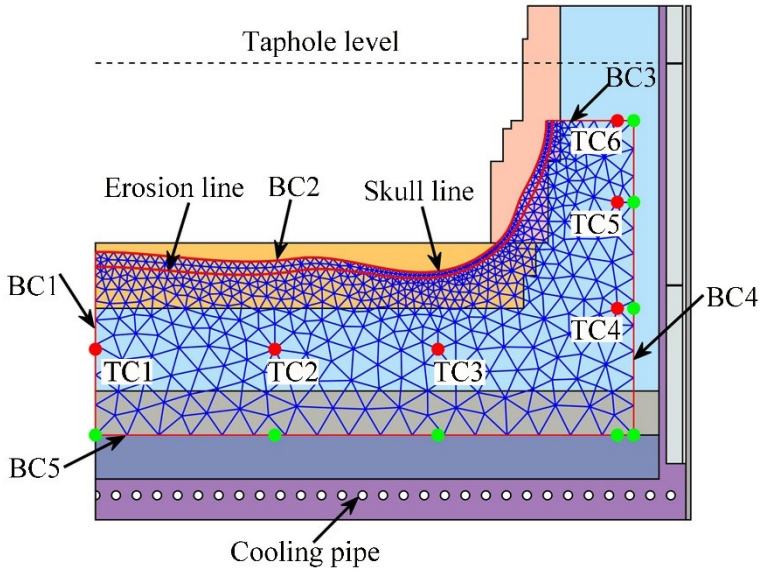

Figure 2. Computational domain (D1) selected on the basis of vertical section S1.

Among the thermocouples denoted by solid dots, TC1-TC6 are located at the reference points and the remaining ones are used to derive the distributions of temperature for the outer and the bottom boundaries. With reference to Figure 2, the boundary conditions

of the heat conduction problem are applied in the following way: the heat fluxes through the rotational axis (BC1) and the upper boundary (BC3) are assumed to be zero, the temperature of the skull line (BC2) is 1150 °C and the temperature distributions of the outer and the bottom boundaries (BC4 and BC5) are interpolated using the readings of the overlying thermocouples.

Special sub-routines are used to pre-process the thermocouple readings that are basically daily mean values. The thermal conductivities of the solid materials of the furnace studied are listed in Table 2. The finite element method and Levenberg-Marquardt algorithm are adopted to calculate the temperature field in each two-dimensional domain (D1-D8) and to tackle the overall inverse problem.

Table 2. Thermal conductivities of the solid materials considered in the hearth wear model

Solid material	Correlation (aT^2+bT+c) [W m^{-1} K^{-1}]		
	a	b	c
Microporous carbon brick	-2×10^{-5}	2.27×10^{-2}	6.06
Super-micropore carbon brick	-1×10^{-5}	1.22×10^{-2}	19.76
Graphite carbon brick	6×10^{-5}	-0.09	107.38
Corundum-mullite brick	1×10^{-6}	-2×10^{-5}	4.21
Mullite brick	3×10^{-6}	-3.90×10^{-3}	6.30
Skull [9, 10, 16]	0	0	2.0

It should, moreover, be stressed that individual calculations for two-dimensional domains usually yield different skull-layer and erosion-zone thicknesses at the rotational axis (cf. Figure 3). In order to address this issue, the thicknesses at the rotational axis are estimated as the mean values of those thicknesses obtained by the individual calculations. After fixing the mean thicknesses at the rotational axis, the

optimization routine is re-run for D1-D8. As illustrated in Figure 3, the two-dimensional results are finally aggregated into a three-dimensional representation (only one half being illustrated for the sake of demonstration) on the basis of cubic spline interpolation.

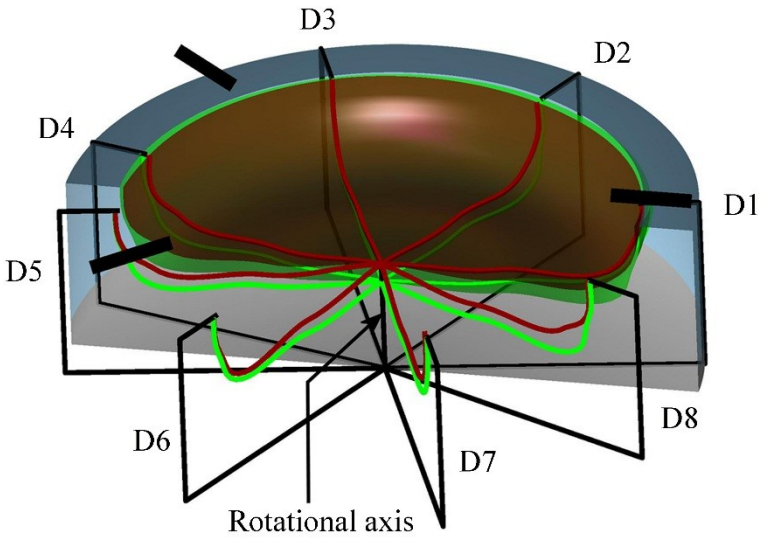

Figure 3. Aggregation of two-dimensional results into a three-dimensional representation (with the tapholes denoted by black bars).

3. Results and Discussion

3.1 Long-term Evolution of Hearth State

To gain an overall picture, time evolutions of key measured data can be studied to extract information about the state of the BF hearth. Figure 4 illustrates the evolutions of (filtered) production rate (panel a) and bottom temperature (panel b) from TC1 (located along the rotational axis in the super-micropore carbon brick, cf. Figure 2) over a span being roughly 2500 days since the blow-in of the BF.

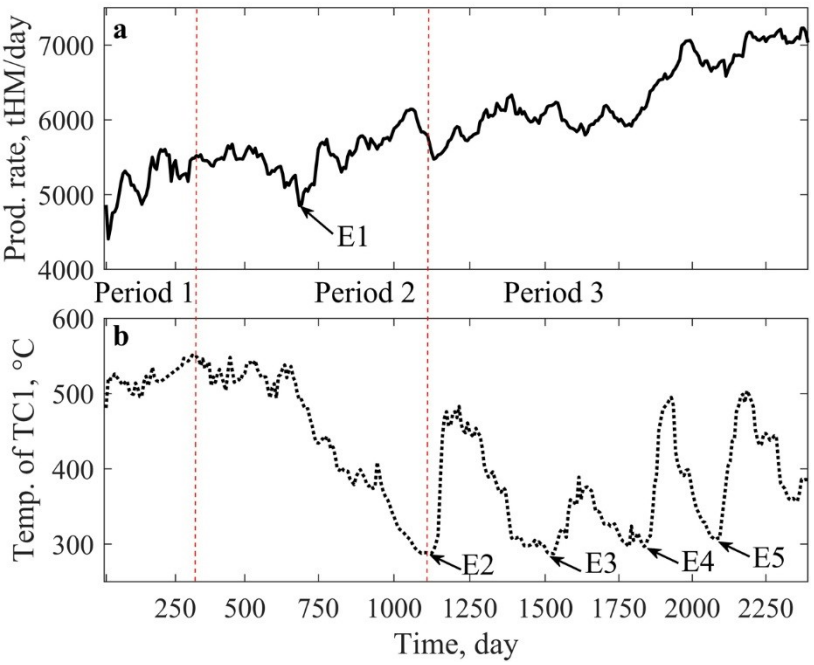

Figure 4. Evolutions of production rate (panel a) and temperature (panel b) from TC1 since the blow-in of the blast furnace.

According to the magnitude of the temperature and its overall trend, the curves in Figure 4 can be divided into three parts that are represented by Periods 1-3. An analysis and discussion of these periods are given below:

- Period 1 corresponds to the initial stage of the furnace campaign during which the production rate is seen to steadily increase and the bottom temperature is generally at a high level. In order to control the bottom temperature, attempts were made to facilitate the formation/growth of skull by increasing the water flow rate of the lowermost cooling pipes (cf. Figure 1a) and thus extracting more heat from the bottom hot face. Still, the bottom temperature ranged between 500 °C and 550 °C. In principle, this can be attributed to the fact that the low-conducting ceramic cup (with a high thermal resistance) plays a dominant role in limiting the heat extracted from the hot face. In the initial stage of the furnace campaign, therefore, it is implied that the thickness of the skull layer is limited and the ceramic cup acts as an ”ectogenous” barrier to avoid direct contact between the carbon-based refractories and the

chemically and mechanically aggressive hot metal. On the other hand, nevertheless, the erosion of the ceramic cup would be inevitably rapid.

- In the middle of Period 2, a scheduled maintenance was carried out, leading to a clear decrease in the production rate (E1 in Figure 4a). After that, the production rate is seen to increase steadily, while the bottom temperature decreases gradually from around 550 °C to 300 °C. It should be mentioned that high temperatures in the hearth sidewall were frequently encountered in the late stage of Period 2 and the grouting techniques were usually adopted. According to Raipala, a decrease in the hearth bottom temperature with an increase in the sidewall temperature is a distinctive symptom indicating an inactive deadman with low permeability in its center zone. [17] It is thought that this argument also holds true for the BF hearth considered here. Under such a circumstance, only a minor fraction of hot metal tends to flow through the center and bottom of the deadman, thus facilitating the formation/growth of skull. However, an inactive deadman is known to be detrimental for the BF operation and should be activated timely. Therefore, measures for activating the deadman were taken in the end of Period 2 (E2 in Figure 4b).
- Period 3 starts with an abrupt increase in the bottom temperature, indicating a successful activation of the deadman. It can be seen in the figure that the production rate steadily increases, while the bottom temperature varies in a cyclic manner and each of the major spikes occurs after taking measures for activating the deadman (as denoted by arrows E3-E5). In practice, the commonly adopted measures for activating the deadman are increasing the coke rate, blast kinetic energy, reducing the coal rate, bottom cooling intensity, adopting central coke charging operation and replacing the upturned tuyere.

As for the gradual deterioration of the deadman state that follows after a successful

activation, the underlying reasons are not yet fully understood. Several earlier investigators have reported similar findings.[9, 17-19] It is believed that the coke and coal rate have a crucial influence on the permeability (especially in the center zone) and floating of the deadman and thus imposes a strong influence on the bottom temperature. In particular, a lower coke rate leads to higher burden density and gravity forces which facilitate a sitting deadman in the hearth where the flow velocities and temperature at the bottom are low.[7, 20-22] A higher coal rate gives rise to a state in the lower furnace where coal fines are consumed slowly, deteriorating the deadman permeability.[17] For substantiating these arguments, the evolutions of bottom temperature (from TC1) and the coke and coal rates during Period 3 are depicted in Figure 5, where it can be observed that the bottom temperature correlates well with the coke and coal rates. In general, the bottom temperature becomes low when the coke rate is low and the coal rate is high.

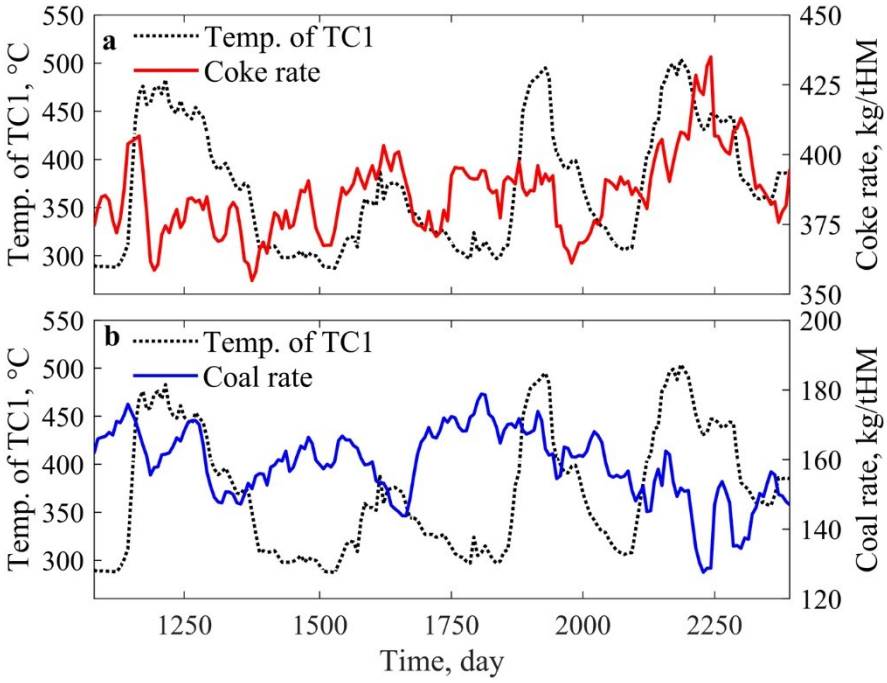

Figure 5. Evolutions of bottom temperature (from TC1, dotted line in panels a and b), coke rate (solid line in panel a) and coal rate (solid line in panel b) during Period 3 (cf. Figure 4).

The wear model was run to estimate the hearth state in terms of internal geometry, and the evolutions of volumes inside the skull line (lower curve) and inside the erosion line (upper curve) are depicted in Figure 6. The difference between the two curves (denoted as a grey region in the figure) thus expresses the total skull volume (in the hearth region considered by the present model). It can be observed in the figure that severe refractory wear only occurs in Period 1 during which the ceramic cup is predicted to be eroded at a high speed (of about 0.54 m^3 $week^{-1}$). After that, the hearth lining refractories experience a comparatively slow long-term erosion (with an average speed of about 0.03 m^3 $week^{-1}$) that primarily takes place at the major peaks of the lower curve (i.e., the skull line). The total skull volume during Period 1 is less than 5 m^3, while during Period 2 and Period 3 it varies in a cyclic manner ranging between 5 m^3 and 50 m^3. It should be pointed out that the skull volume is derived based on the blast furnace structure and operational conditions considered in the current work. Under different conditions such as the hearth size and the iron ore as well as coke quality, the skull volume could vary.

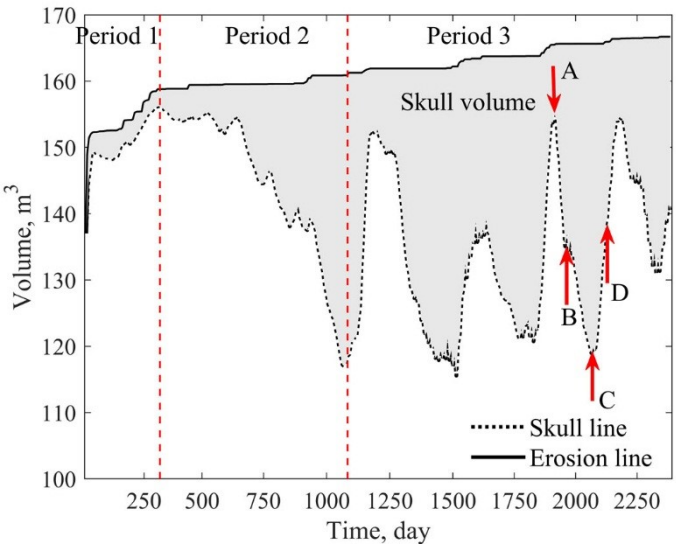

Figure 6. Evolutions of volumes inside the skull line (lower curve) and inside the erosion line (upper curve).

Careful inspection also reveals that the evolution of the lower curve in Figure 6 shows a marked resemblance to that of the bottom temperature in Figure 4b. It is therefore presumed that a major portion of the skull is formed at the bottom of the hearth where the liquid velocities are generally low. Moreover, as mentioned earlier, the content of Ti in the feedstock of the BF is around 0.5%, which may lead to the formation of a high-viscosity film in the vicinity of the bottom hot face, which suppresses the local iron flow to a noticeable extent.[23, 24]

3.2 Detailed Analysis of Modelling Results

In order to shed more light on the typical hearth behavior, three-dimensional and the associated two-dimensional pictures of the hearth inner geometry are provided in the left and right columns of Figure 7, respectively. Panels a-b represent four snapshots taken at and after the third spike during Period 3 (denoted with vertical arrows A-D in Figure 6). In the left column, the colors express the thickness of skull layer and range from blue (skulled) to red (eroded). In each panel, moreover, the two-dimensional picture on the right is in fact the vertical section along the line of TH1.

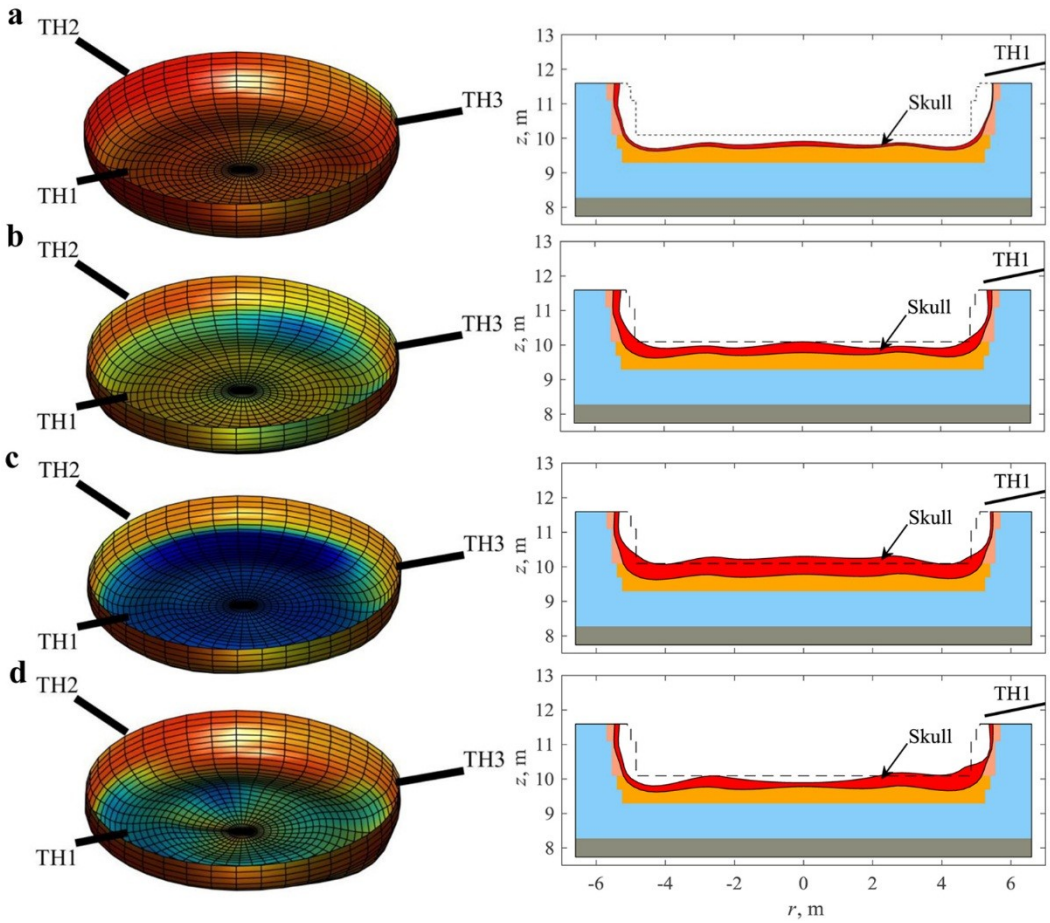

Figure 7. Three-dimensional (left column) and the associated two-dimensional (right column) pictures of the hearth inner geometry for typical cases.

In Figure 7, panel a depicts an eroded hearth where the bottom and sidewall of the ceramic cup are eroded to a high extent, and the skull layer is thin. Since a severely eroded ceramic cup as well as a thin skull layer correspond to a low thermal resistance of the heat transfer system, the formation/growth of skull is facilitated with the aid of enhanced cooling from the cold face. Thus, the skull layer covering the ceramic cup gradually becomes thicker as observed in panel b, where the skull layer distribution is seen to be fairly uniform except for regions beneath each taphole. In panel c, the skull on the hearth bottom seems to accumulate further and its upper surface even exceeds the height of the original ceramic cup (dashed line), while less skull appears on the sidewall. This is basically attributed to an inactive deadman with low permeability in its center zone. Under such a circumstance, the overall iron flow in the hearth is

peripheral. In panel d, the skull layer is found to become thinner, especially in the bottom region due to an activation of the deadman: an active deadman (with relatively uniform permeability) allows hot metal to flow across its center and bottom, thus increasing the liquid-solid heat transfer coefficient, leading to dissolution of the skull. Moreover, it is worth noticing in Figure 7 that the skull layer distribution is fairly uniform in the angular direction of the hearth sidewall, compared to the results reported by Brännbacka and Saxén for a one-taphole BF with an inner volume being approximately 1000 m^3.[9] In order to explain this observation, the role of alternative tapping using the three tapholes is believed to be of crucial importance.

The estimated hearth wear states along the lines of TH1-3 of the case corresponding to the vertical arrow D in Figure 6 are further depicted in Figure 8. It can be observed that erosion lines in the three vertical sections are quite similar especially in the bottom of the hearth. After running for about 6 years the 0.8-meter thick ceramic pad is seen to be eroded by about 0.3 m, the 0.7-meter thick ceramic cup is seen to be eroded by about 0.5 m. Thus, it may conclude that lining wear of the BF hearth mainly occurs at the sidewall, where due attention should be paid to how to prevent excessive lining erosion.

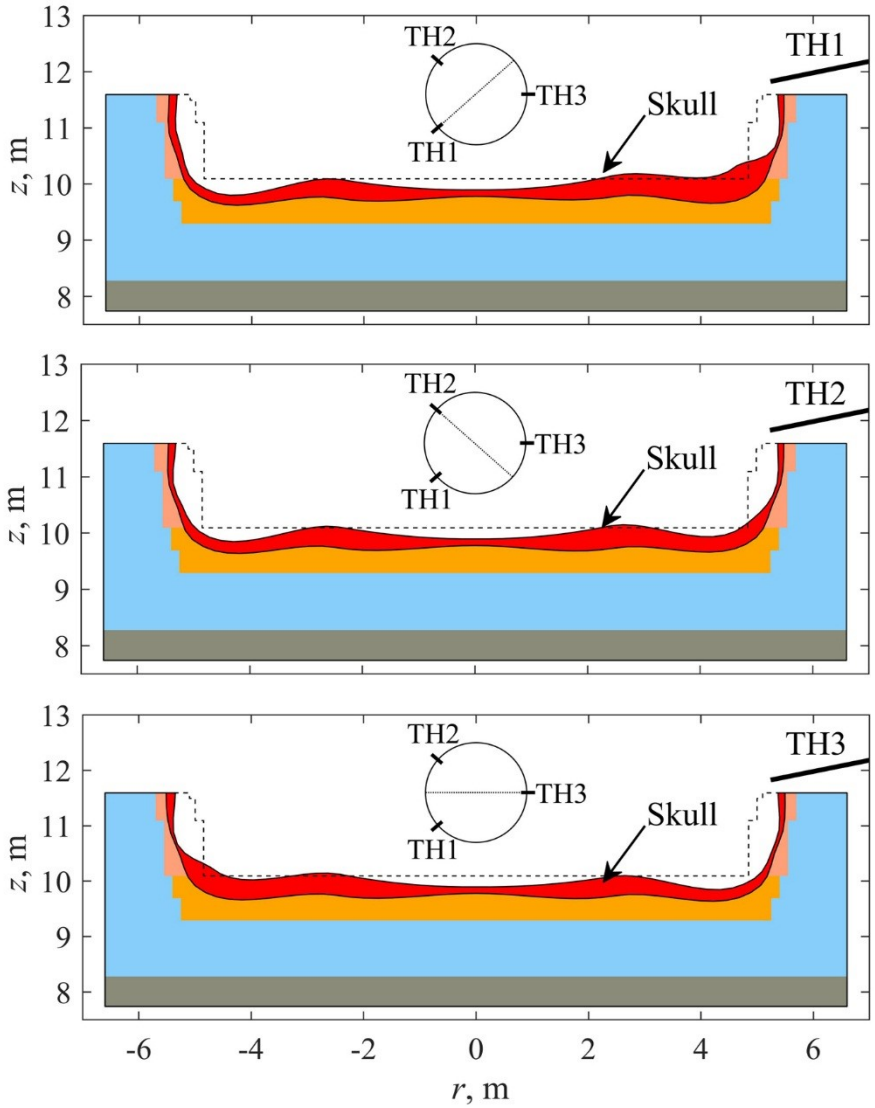

Figure 8. Estimated hearth wear states along the lines of TH1-3 of the case corresponding to the vertical arrow D in Figure 6.

In the BF operation, it is commonly known that a high production rate with a short taphole will promote the existence of annular-shaped bypass flows along the sidewall in the vicinity of the taphole and consequently give rise to an excessive local erosion.[25-28] It is therefore desirable to keep the taphole as long as possible to move the region with high flow velocities towards the hearth center, which will facilitate the formation/growth of skull with the aid of enhanced cooling from the cold face. Thus, prolonging the taphole is probably the fastest and most effective way to control abnormal and excessive erosion at the hearth sidewall. For this reason, attempts were

made in the BF by blanking 1-2 tuyeres above the taphole in use for some period of time. Under such a circumstance, the local inflow of hot metal is reduced and a possible local floating of the deadman below the taphole level is suppressed.[25] A good contact between the injected mud and the deadman, which is a prerequisite for achieving a long taphole, is therefore expected. In order to emphasize the importance of a long taphole, Figure 9 illustrates comparisons of the length of TH1 (measured drill depth) and the average estimated thickness of the skull layer in the sidewall region bounded by S5 and S6 (see the insert in Figure 9). The time span corresponds to Period 3 (Figure 4). It is found that a thicker skull layer correlates well with a longer taphole. This clear correlation between the measured and predicted quantities also confirms the validity of the present hearth wear model.

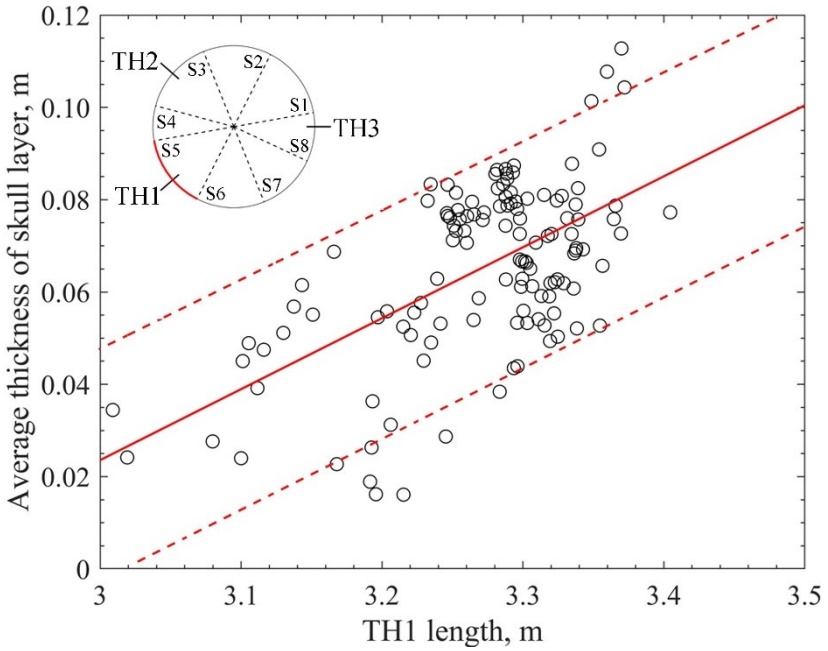

Figure 9. Comparisons of TH1 length and the average thickness of the skull layer in the sidewall region bounded by S5 and S6.

4. Conclusions and Future Work

In order to provide an overall picture of the hearth internal geometry of a large BF in a Chinese steelworks, a wear model was developed based on an inverse heat-conduction

problem, to track the evolutions of erosion and skull lines in the hearth. Special emphasis was also put on the problem formulation to yield a fast and robust model that can be used routinely to assess the state of the hearth. The paper has presented an analysis of the overall operation of the hearth during the time period studied and a more detailed scrutiny of certain events in the operation, where major changes in the hearth state was detected by the wear model. The validity of the wear model was confirmed based on a clear correlation found between the measured taphole length and average thickness of the estimated skull layer. The main findings of the present work can be summarized as:

(1) During the initial stage of the furnace campaign, the low-conducting ceramic cup (with a high thermal resistance) limits the heat extracted from the hot face. Therefore, the thickness of the skull layer is limited and the ceramic cup acts as an 'ectogenous' barrier to avoid direct contact between the carbon-based refractories and the chemically and mechanically aggressive hot metal.

(2) As the ceramic cup is gradually eroded, a skull layer with a volume ranging between 5 m^3 and 50 m^3 is formed in the hearth. In general, the skull-layer distribution is fairly uniform in the angular direction of the hearth sidewall and the skull layer in the bottom of the hearth is much thicker than that at the sidewall. Therefore, lining erosion of the hearth mainly occurs in the sidewall, where due attention should be paid to prevent excessive consumption of the lining materials.

(3) A thicker skull layer preventing the sidewall from excessive lining erosion correlates well with a longer taphole. Therefore, prolonging the taphole plays a key role in retaining the hearth integrity and thus prolonging the BF campaign.

In forthcoming work, the hearth wear model will be applied to process data from other industrial blast furnaces. Since it is possible to collect the thermocouple signals on a

minute basis, attempts will also be made to use the time-dependent formulation of the heat conduction equation in order to investigate the dynamics of rapid changes in the hot face conditions. Future work will also be focused on a possible combination of the wear model results with the findings from big data techniques in order to shed light on the complicated interaction between the hearth variables, i.e., liquid flow patterns, deadman state and internal geometry.

Acknowledgements

The authors would like to express their gratitude to the National Science Foundation of China (Grants 51604068, 51574064), for financially supporting this work.

Conflict of Interest

The authors declare no conflict of interest.

References

[1] H. B. Lüngen, P. Schmöle, *Steel Res. Int.* **2020**, *91*, 2000182.

[2] K. X. Jiao, J. L. Zhang, Q. F. Hou, Z. J. Liu, G. W. Wang, *Steel Res. Int.* **2017**, *88*, 1600475.

[3] L. Shao, Q. L. Xiao, C. B. Zhang, Z. S. Zou, H. Saxén, *Processes **2020***, *8*, 1335.

[4] L. Shao, C. B. Zhang, Y. X. Qu, H. Saxén, Z. S. Zou, *Steel Res. Int.* **2020**, *91*. 1900460.

[5] Y. F. Zhao, D. Fu, L.W. Lherbier, Y. Chen, C.Q. Zhou, J.G. Grindey, *Steel Res. Int.* **2014**, *85*, 891.

[6] L. Shao, P. Taskinen, A. Jokilaakso, H. Saxén, Y. X. Qu, Z. S. Zou, *Steel Res. Int.* **2019**, *90*, 1800297.

[7] K. Andreev, G. Louwerse, T. Peeters, J. van der Stel, *Ironmak. Steelmak*. **2017**, *44*, 81.

[8] J. Torrkulla, H. Saxén, *ISIJ Int.* **2000**, *40*, 438.

[9] J. Brännbacka, H. Saxén, *Ind. Eng. Chem. Res*. **2008**, *47*, 7793.

[10] M. Zagaria, V. Dimastromatteo, V. Colla, *Ironmak. Steelmak.* **2010**, *37*, 229.

[11] H. B. Zhao, S. F. Huo, S. S. Cheng, *Int. J. Miner. Metall. Mater*. **2013**, *20*, 345.

[12] Y. Kaymak, H. Bartusch, T. Hauck, J. Mernitz, H. Rausch, R. Lin, *Steel Res. Int.* **2020**, *91*, 2000055.

[13] C. M. Chang, W. T. Cheng, C. E. Huang, S. W. Du, *Int. Commun. Heat Mass Transfer* **2009**, *36*, 480.

[14] H. B. Vogelpoth, G. Still, M. Peters, *Stahl Eisen* **1985**, *105*, 451.

[15] T. Inada, A. Kasai, K. Nakano, S. Komatsu, A. Ogawa, *ISIJ Int.* **2009**, *49*, 470.

[16] M. Swartling, B. Sundelin, A. Tilliander, P.G. Jönsson, *Steel Res. Int.* **2010**, *81*, 186.

[17] K. Raipala, *Dr. Thesis*, Helsinki University of Technology, Finland, **2003**.

[18] R. J. Nightingale, *Dr. Thesis*, University of Wollongong, Australia, **2000**.

[19] M. Helle, H. Saxén, O. Kerkkonen, *Steel Res. Int.* **2009**, *80*, 384.

[20] B. Y. Guo, D. Maldonado, P. Zulli, A. B. Yu, *ISIJ Int.* **2008**, *48*, 1676.

[21] B. Y. Guo, A. B. Yu, P. Zulli, D. Maldonado, *Steel Res. Int.* **2011**, *82*, 579.

[22] X.F. Dong, P. Zulli, *Ironmak. Steelmak.* **2020**, *47*, 307.

[23] K.M. Komiyama, B. Y. Guo, H. Zughbi, P. Zulli, A. B. Yu, *Steel Res. Int.* **2015**, *86*, 592.

[24] K. Gao, K. Jiao, J. Zhang, L. Zhang, C. Wang, W. Gong, J. Zheng, H. Zhang, *ISIJ Int.* **2020**, *60*, 2385.

[25] N. Tsuchiya, T. Fukutake, Y. Yamauchi, T. Matsumoto, *ISIJ Int.* **1998**, *38*, 116.

[26] A. Shinotake, H. Nakamura, N. Yadoumaru, Y. Morizane, M. Meguro, *ISIJ Int.* **2003**, *43*, 321.

[27] Y. Matsui, R. Tadai, K. Ito, T. Matsuo, N. Nagai, T. Imai, *ISIJ Int.* **2005**, *45*, 1439.

[28] L.R. Nelson, R.J. Hundermark, *J. S. Afr. Inst. Min. Metall.* **2016**, *116*, 465.